

Far-IR dust properties of highly dust obscured AGNs from the *AKARI* and *WISE* all-sky surveys

ANSON LAM,¹ MATTHEW MALKAN,¹ AND EDWARD WRIGHT¹

¹*Physics and Astronomy Department, University of California, Los Angeles, CA 90095-1547, USA*

ABSTRACT

The combination of the *AKARI* and *WISE* infrared all-sky surveys provides an unique opportunity to identify and characterize the most highly dust obscured AGNs in the universe. Dust-obscured AGNs are not easily detectable and potentially underrepresented in extragalactic surveys due to their high optical extinction, but are readily found in the *WISE* catalog due to their very red mid-IR colors. Combining these surveys with photometry from *Herschel* SPIRE and SDSS, we use SED modeling to characterize the extinction and dust properties of these mid-IR selected AGNs. We show that we can estimate bolometric corrections for dusty AGNs using *WISE* colors. Using *AKARI*'s far-IR wavelength photometry and broadband AGN/galaxy spectral templates, we also estimate the mass and temperature properties of our AGN sample.

Keywords: infrared: galaxies - Galaxies: active - catalogs

1. INTRODUCTION

The all-sky coverage of the *WISE* and *AKARI* infrared surveys allows for a large scale study of dust-obscured AGNs. The IR wavelength range spanned by these photometric surveys also represents the bulk of the bolometric luminosity for dusty galaxies. Using this photometry, we can identify and determine the physical properties of these dusty AGNs without the need for time-intensive spectroscopy. Dust modeling in the IR requires taking into consideration factors such as dust composition, emissivity, orientation, etc., but we show that this can be done using relatively simple SED models. We describe our AGN sample selection criteria in Section 2. In Section 3, we use optical photometry and SED templates to quantify optical dust obscuration and the mid-IR flux contribution of the AGN component. Since far-IR data is relatively scarce compared to shorter wavelength data, we show that we can derive bolometric corrections based on mid-IR photometry in Section 4. Using the far-IR photometry available to us, we examine the physical properties of AGN dust in Section 5.

2. DATA AND AGN SELECTION

We combine photometric data from the following catalogs: AllWISE Catalog (3.4, 4.6, 12, and 22 μm ; Wright et al. 2010), *AKARI* Bright Source Catalog (65, 90, 140, and 160 μm ; Kawada et al. 2007), *Herschel* SPIRE (250, 350, and 500 μm ; Griffin et al. 2010), SDSS (*ugriz*; Abazajian et al. 2009). We identify AGN candidates using a *WISE* color-cut criterion $W1 - W2 > 0.8$, which selects mid-IR AGNs with high completeness and reliability, and includes both optically unobscured and obscured AGNs (Stern et al. 2012). Figure 1 summarizes our selection process and final number counts. For redshifts, we use the 2MASS Photometric Redshift catalog (Bilicki et al. 2014), which contains a million galaxies with an accuracy of $\sigma = 0.015$ and a median redshift of $z \sim 0.1$.

3. OPTICAL SED MODELING

Using low-resolution spectral templates (Assef et al. 2010), we model each quasar as a linear combination of an AGN template and a single galaxy template (spiral, elliptical or irregular). We apply optical extinction curves (Gordon & Clayton 1998; Cardelli et al. 1989) to the SED fit to simulate the effects of obscuration, and quantify this using the $E(B - V)$ extinction. Since they are derived from dustless galaxies, these templates systematically underpredict the *WISE* W3 and W4 fluxes in the mid-IR. We observe no correlation between $E(B - V)$ and this mid-IR flux discrepancy, suggesting that the mid-IR continuum is not simply due to the absorbed and reprocessed optical/UV emission. This also suggests that optical obscuration is dependent on other factors such as dust geometry, orientation, distribution, etc. Our SEDs also show

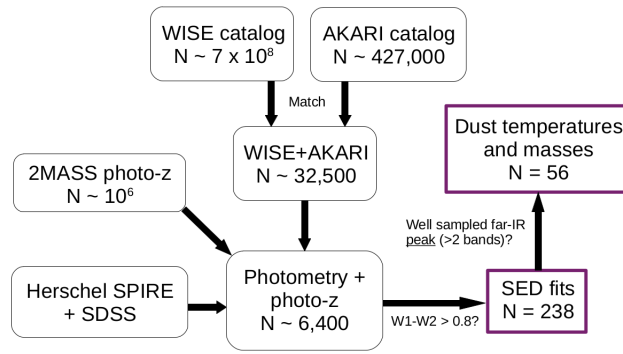


Figure 1. Flowchart outlining the AGN selection criteria.

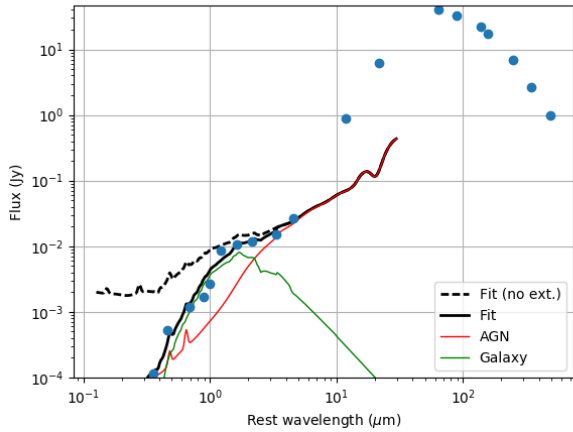


Figure 2. SED fit for $\lambda < 10 \mu\text{m}$ using the templates from Assef et al. (2010) (red and green curves). The solid curve shows the sum of the templates with extinction applied, while the dashed curve shows the model without extinction.

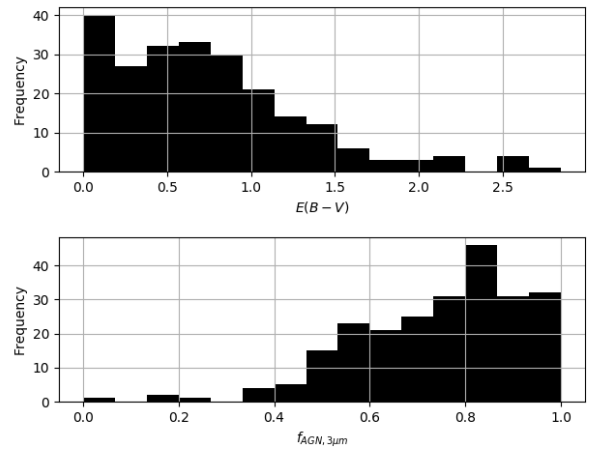


Figure 3. [Top] Distribution of optical $E(B - V)$ extinction values derived from SED fitting using the templates of Assef et al. (2010). [Bottom] Distribution of the fractional AGN contribution to the total luminosity for $\lambda = 3 \mu\text{m}$.

that most of the objects in our sample have the majority of their flux density at $3 \mu\text{m}$ coming from the AGN component. Figure 2 shows an example AGN SED, with histograms of $E(B - V)$ and $f_{\text{AGN},3\mu\text{m}}$ shown in Figure 3.

4. IR BOLOMETRIC CORRECTIONS

In addition to the templates from Assef et al. (2010), we fit the far-IR SEDs using templates from Mullaney et al. (2011) and measure the bolometric luminosity for $< 1000 \mu\text{m}$. Since Assef et al. (2010) and Mullaney et al. (2011) treat mid-IR dust emission differently, we join the two template sets using a mid-IR power law. By integrating the SED at different long wavelength cutoffs, we can determine the fraction of F_{bol} represented below a certain wavelength (Figure 4). In Figure 5 we show that the fraction of the bolometric flux at $< 25 \mu\text{m}$ is negatively correlated with $W2 - W4$.

5. DUST TEMPERATURES AND MASS FRACTIONS

We use two different models to fit the mid to far-IR dust emission:

a) A modified blackbody function with emissivity factor $\beta = 2$ to model the cold dust emission, and a power-law term (with an exponential cutoff) to account for the mid-IR dust emission due to AGN heating (Casey 2012):

$$S_{\nu}(\lambda) = A_{\text{BB}} \frac{\lambda^{-(\beta+3)}}{e^{hc/\lambda kT} - 1} + A_{\text{PL}} \lambda^{\alpha} e^{-(\lambda/\lambda_0)^2}. \quad (1)$$

b) A temperature power-law distribution of the form $dM/dT \propto T^{\gamma}$ with a low temperature cut-off T_c to represent all the dust temperature components (Kovács et al. 2010). This distribution is used to weight the modified blackbody function, which is integrated over all temperatures to get the resultant flux density:

$$S_\nu(\gamma, T_c) \propto \int_{T_c}^{\infty} \nu^\beta B_\nu(T) T^{-\gamma} dT. \quad (2)$$

Figure 6 shows the resultant fits of Equations (1) and (2) to an example SED. We measure a median value of $\langle \gamma \rangle \sim 8$, which is consistent with a small warm dust fraction and a spatially diffuse dust distributed at farther distances from the central engine. A more compact dust distribution would have values around $\gamma \sim 4-5$, which corresponds to a larger fraction of dust at closer radii and thus higher temperatures. Although the torus surrounding the central AGN engine is believed to be compact, large values of γ can result if this torus can be embedded within a larger, extended dust distribution. In Figure 7, we show there is also a strong correlation between γ and $W2 - W4$ color, which shows that the temperature and spatial dust distribution are directly measurable. The total dust mass is given by:

$$M_d \propto \frac{A_d}{\kappa_0} \int_{T_c}^{\infty} T^{-\gamma} dT, \quad (3)$$

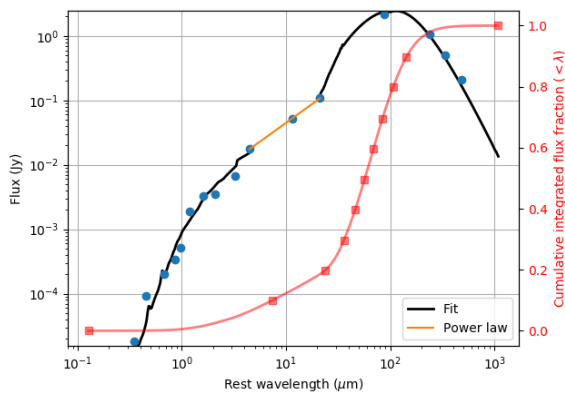


Figure 4. An example of a bolometric SED fit. The black curve shows the best template fit and the yellow curve is the power law continuum that we fit between the W2 and W4 bands. The red curve shows the cumulative integrated flux (ranging from the lower limit of the SED, up to the corresponding wavelength) as a fraction of F_{bol} . Red squares denotes increments of 0.1 along the vertical axis.

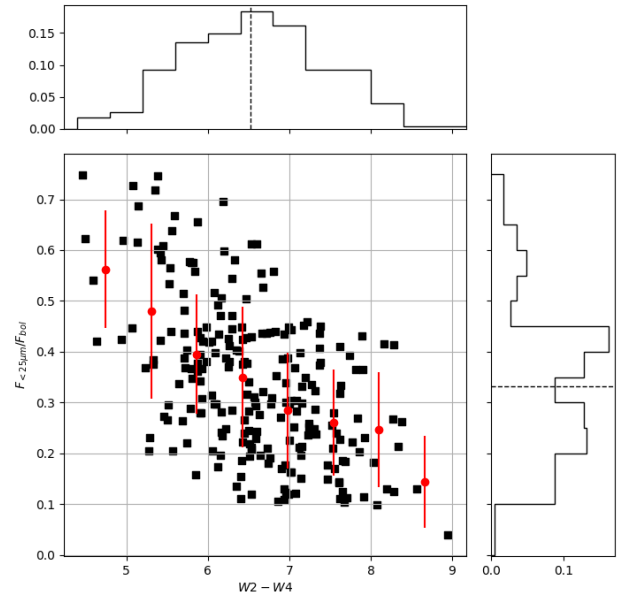


Figure 5. The fraction of the bolometric luminosity below $25 \mu\text{m}$ plotted against $W2 - W4$ color.

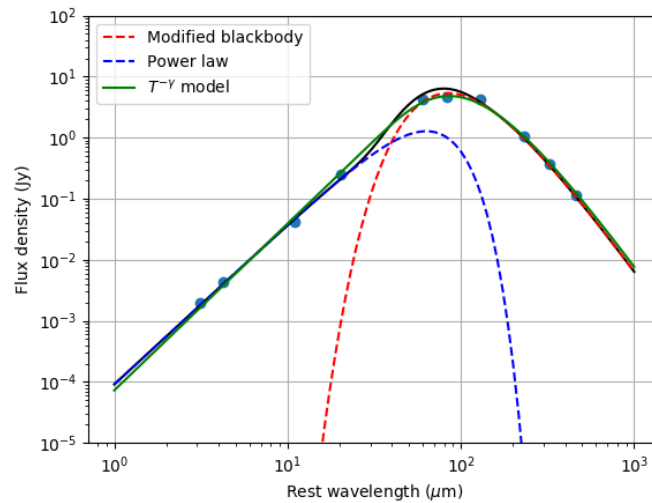


Figure 6. An example SED with the far-IR emission fit using Equation 1 (black curve), which is the sum of a single temperature blackbody (red dashed curve) and a exponentially attenuated mid-IR power law (blue dashed curve). The green curve shows the fit using Equation 2

where κ_0 is the opacity and A_d is the total area of the individual dust grains added together. Since these parameters tend to be highly uncertain, we compute mass ratios of dust temperature components instead of the absolute dust mass. We define the warm dust mass fraction temperature cutoff to be $T_c = 50$ K, and $T_c = 15$ K for the total dust. In Figure 8, we show that there exists a positive trend between the fractional AGN contribution to the integrated flux at $< 30 \mu\text{m}$ and warm dust mass fraction, suggesting that AGN activity is primarily responsible for heating the warm dust.

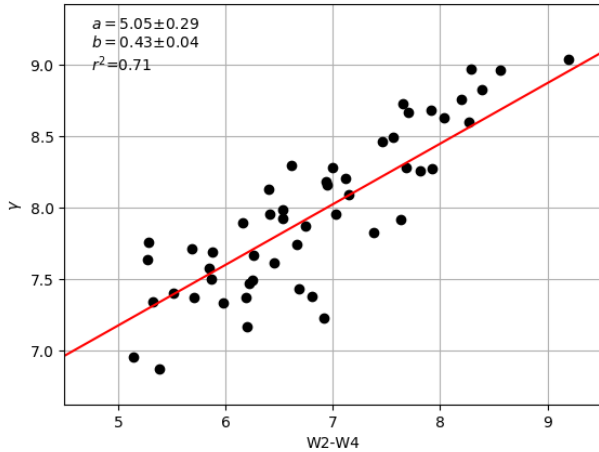


Figure 7. Correlation between α (mid-IR continuum power law index Equation 1) and γ (temperature distribution power law index in Equation 2)

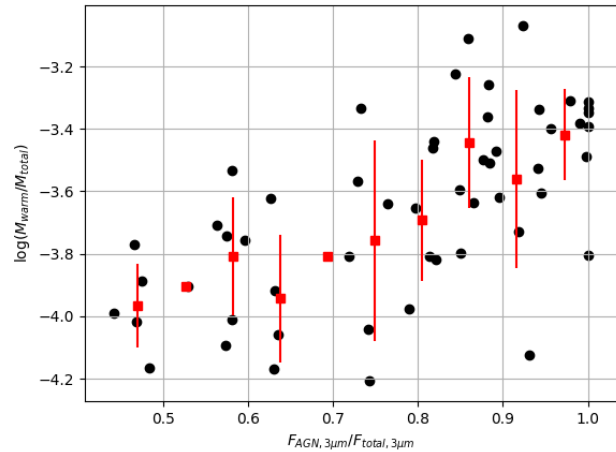


Figure 8. Warm dust fraction plotted against the AGN contribution to the total flux for $\lambda < 30 \mu\text{m}$. Red squares and error bars denote means and standard deviations of their respective bins.

6. CONCLUSIONS

Using only archival photometric data and simple SED models, we've demonstrated that we can identify and understand the physical properties of dust-obscured AGNs that have sufficient far-IR photometry and redshift data. Optical SED modeling confirms that *WISE*-selected AGNs have a range of obscurations between $0 < E(B - V) < 1.5$ and contain a significant AGN component. By comparing *WISE* photometric colors, we can estimate the bolometric correction to the integrated total optical and mid-IR flux of an AGN. Using simple models with only 3–4 parameters, we can quantify dust temperature, mass, and spatial distribution using only photometric data.

ACKNOWLEDGMENTS

This research is based on observations with AKARI, a JAXA project with the participation of ESA. This publication makes use of data products from the Wide-field Infrared Survey Explorer, which is a joint project of the University of California, Los Angeles, and the Jet Propulsion Laboratory/California Institute of Technology, funded by the National Aeronautics and Space Administration.

REFERENCES

- Abazajian, K. N., Adelman-McCarthy, J. K., Agüeros, M. A., et al. 2009, *ApJS*, 182, 543
 Assef, R. J., Kochanek, C. S., Brodwin, M., et al. 2010, *ApJ*, 713, 970
 Bilicki, M., Jarrett, T. H., Peacock, J. A., Cluver, M. E., & Steward, L. 2014, *ApJS*, 210, 9
 Cardelli, J. A., Clayton, G. C., & Mathis, J. S. 1989, *ApJ*, 345, 245
 Casey, C. M. 2012, *MNRAS*, 425, 3094
 Gordon, K. D., & Clayton, G. C. 1998, *ApJ*, 500, 816
 Griffin, M. J., Abergel, A., Abreu, A., et al. 2010, *A&A*, 518, L3
 Kawada, M., Baba, H., Barthel, P. D., et al. 2007, *PASJ*, 59, S389
 Kovács, A., Omont, A., Beelen, A., et al. 2010, *ApJ*, 717, 29
 Mullaney, J. R., Alexander, D. M., Goulding, A. D., & Hickox, R. C. 2011, *MNRAS*, 414, 1082
 Stern, D., Assef, R. J., Benford, D. J., et al. 2012, *ApJ*, 753, 30
 Wright, E. L., Eisenhardt, P. R. M., Mainzer, A. K., et al. 2010, *AJ*, 140, 1868